Three-dimensional optical imaging of microvascular networks within intact lymph node *in vivo*

Yeongri Jung,* Zhongwei Zhi,* and Ruikang K. Wang
Oregon Health & Science University, Department of Biomedical Engineering 3303 SW Bond Avenue, Portland, Oregon 97239

Abstract. Sentinel lymph nodes (SLNs) are the first lymph nodes to drain wastes originated from cancerous tissue. There is a need for an *in vivo* imaging method that can image the intact SLN to further our understanding of its normal as well as abnormal functions. We report the use of ultrahigh sensitive optical microangiography (UHS-OMAG) to image functional microvascular and lymphatic vessel networks that innervate the intact lymph node in mice *in vivo*. The promising results show a potential role of UHS-OMAG in the future understanding and diagnosis of the SLN involvement in cancer development. [DOI: 10.1117/1.3496301]

Keywords: lymph node; optical microangiography; lymphangiography; lymphatic morphology; blood flow.

Paper 10375LR received Jul. 3, 2010; revised manuscript received Aug. 31, 2010; accepted for publication Sep. 2, 2010; published online Oct. 6, 2010.

The lymphatic system is one of the key constituents in the human immune system that plays a significant role for metastatic dissemination of malignancies. It consists of multiple lymphoid tissue structures (lymph nodes) interconnected by a network of lymph vessels through lymph circulation. The lymph nodes (LNs) entrap foreign, potentially harmful substances such as bacteria and cancer cells that travel through the human body via blood and lymph carriers. The first lymph nodes receiving drainage from a tumor are called sentinel lymph nodes (SLNs). Currently, SLN biopsy has become the preferred method for axillary lymph node staging of breast cancer patients with clinically negative axillary lymph nodes.[1] If the outcome of SLN biopsy is positive, then the breast lesions of concern are most likely metastatic. The procedure of SLN biopsy requires the removal of full axillary lymph nodes, with the help of an invasive use of blue dyes, for histological assessment.[2] If pathologic results for SLNs are negative, then it is not necessary to dissect the full axillary lymph nodes, because the outcome from the SLN alone can achieve a firm diagnosis with success rates of 90 to 97%.[2] In addition, this invasive SLN biopsy procedure, although clinically effective, would potentially result in postoperative complications, e.g., lymphedema, sensory nerve injury, seroma formation, etc.[3] Consequently, a noninvasive or minimally invasive imaging technique that can provide functional information of the SLN would represent a significant advance in the clinical diagnosis of metastatic cancers.

Optical imaging techniques are increasingly being used in the clinical environment, allowing for improved screening and diagnosis while minimizing the number of invasive procedures. Among them, photoacoustic (PA) imaging has recently attracted much attention, with hopes that it may provide a useful alternative to the current SLN biopsy.[4] PA relies on transient light absorption and subsequent detection of acoustic emission to achieve imaging. With the help of exogenous contrast agents, PA imaging has been reported to identify rat SLNs *in vivo*.[5] However, its relatively low spatial resolution ($>\sim 100\ \mu$m) currently limits its imaging capability at the lymph node organ level.

To further improve our understanding of the physiological functions of the LNs, what is needed is an imaging technique capable of visualizing its detailed morphology, as well as the blood and lymph microcirculations that supply the LN. In this regard, optical coherence tomography (OCT) has recently been reported for high resolution 3-D visualization of lymph node morphology.[6,7] The reported *ex-vivo* OCT imaging results were shown morphological structures that corresponded well with histological features of the LNs, suggesting the potential of OCT to visualize LN microstructures on a scale of micrometastases, and to detect metastatic nodal diseases intraoperatively. However, these morphological studies detected no significant differences between the OCT images of LNs from tumor-bearing animals and those from control animals.[6] Notwithstanding, there is no imaging technique available to date that can provide the 3-D information of microcirculation that supplies the lymphatic tissue *in vivo*.

Being a novel extension of OCT, optical microangiography (OMAG)[8] is a recently developed imaging technique capable of producing 3-D images of dynamic blood perfusion within microcirculatory tissue beds with an imaging depth of $\sim$2 mm. OMAG is a label-free technique, because it uses the endogenous light scattering from flowing blood cells within patent vessels to produce the imaging contrast. An unprecedented sensitivity to the blood flow down to 4 μm/s was reported with the most recent development of ultrahigh sensitive OMAG (UHS-OMAG).[9] With such high sensitivity to the flow, the modality has been successfully employed to image the microcirculations within tissue beds of small animals[10] and has also extended to human studies such as skin[9] and eye.[11] In this work, we approach the feasibility of UHS-OMAG to image the 3-D blood vessel networks in the LNs of mice *in vivo*.

The UHS-OMAG system setup used in this study is similar to the one used in our previous work.[10] Briefly, the setup was operating at 1310-nm wavelength with a spatial resolution of $\sim 9\ \mu$m (x-y-z) in biological tissue. The system has an imaging depth of 2.22 mm in biological tissue and a sensitivity of 105 dB measured at the focal spot ($\sim$0.5 mm below the zero delay line). The total loss of system sensitivity was measured to be less than 15 dB at 2.00 mm. The sensitivity of the system to the blood flow ranged from $\sim 4\ \mu$m/s to ~ 22.2 mm/s,[9] which we expect is sufficient to image the blood vessel networks within the lymph nodes. When imaging, we rapidly scanned the probe beam over the sample,

*These authors contributed equally to this work.
Address all correspondence to Ruikang K. Wang. Tel: 503-418-9317; Fax: 503-418-9311; E-mail: r.k.wang@bme.ogi.edu.

1083-3668/2010/15(5)/050501/3/$25.00 © 2010 SPIE

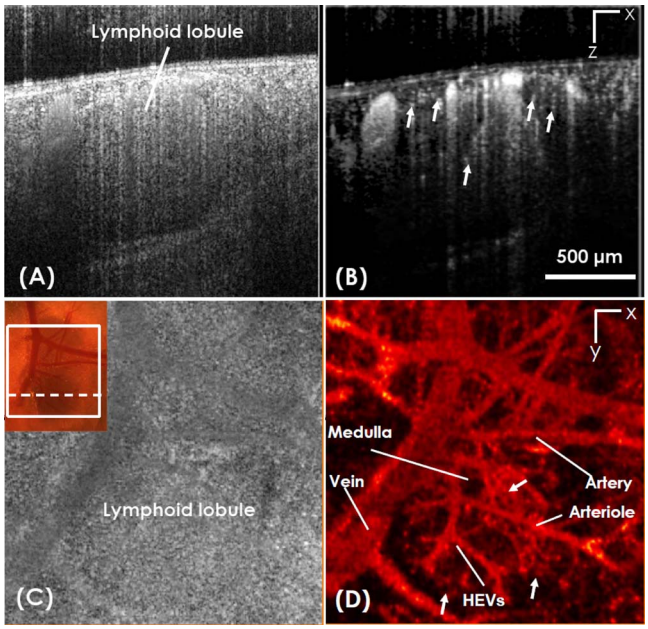

Fig. 1 UHS-OMAG images of depth-resolved microstructures and microcirculation network within an axillary lymph node *in vivo*. The insert in the upper left corner in (c) is the photograph of the sample in which a bean-shaped axillary lymph node is situated, where the white box indicates the region scanned by OMAG. The top images show (a) a typical cross sectional microstructure and (b) the corresponding blood flow images at the location indicated by the dashed line in the photograph. The bottom images show the enface images of (c) the microstructures and (d) the corresponding blood vessels, extracted from the 3-D optical dataset. The results show the morphological features as well as the microvascular network within the lymph node. (scale bar = 500 μm).

while the spectrometer was continuously recording the OMAG signals formed between the reference and the sampling light at an imaging speed of 47,000 depth scans (A-scans) per second. With this imaging speed, we acquired 256 A-scans in the x direction (B-scan) of 1.8 mm to form one cross sectional image (B frame). This configuration determined the system frame rate at 180 frames per second (fps). In the y direction, we captured a high density C-scan (i.e., y direction scan), consisting of 1500 B-scans over 1.8 mm. Accordingly, it required ~8 sec to acquire a complete 3-D data volume of $1.8 \times 1.8 \times 2.22$ mm^3. Then, a UHS-OMAG algorithm[9] was applied to this 3-D dataset to obtain morphological and microcirculatory images of the scanned tissue volume.

To demonstrate the ability of UHS-OMAG imaging of the LN vascular networks *in vivo*, three-month-old C57 BL/6 mice (26 to 30 g) were used. All experimental animal procedures were performed in conformity with the guidelines of the United States National Institutes of Health. During imaging, the mouse was immobilized in a stereotaxic stage and was anesthetized with vaporized isoflurane (0.2 L/min oxygen and 0.8 L/min air). The body temperature was kept at 37 °C with use of a heating pad. For imaging, the axillary lymph nodes were exposed by pulling aside the skin and surrounding tissues. Then, the mouse was positioned under the scanning probe, with the lymph node carefully placed within the depth

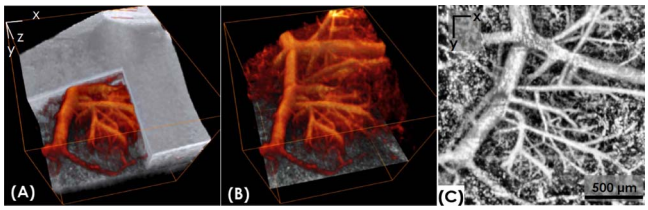

Fig. 2 UHS-OMAG visualizes 3-D morphology and microvascular network within an axillary lymph node. Shown are (a) the merged view of volumetric microstructures and blood vessels, where a cut-away view of the microstructural volume gives an appreciation of how blood vessels innervate this lymphatic tissue; (b) the volumetric visualization of the blood vessel network alone; and (c) the x-y projection view of the blood vessels shown in (b). The volume size is $2.0 \times 2.0 \times 1.5$ mm^3 (x-y-z) in (a) and (b).

of focus of the probe beam, as monitored by real-time OMAG/OCT structural images on the fly.

The imaging results for one LN are shown in Fig. 1. A photograph of the sample is given by the insert in the upper left corner of Fig. 1(c) where the white box indicates the region scanned by the UHS-OMAG system. The size of the oval lymph node was about 1×1.5 mm. One advantage of the OMAG modality is that it is capable of providing the depth-resolved tissue structural image and the coregistered blood flow image in parallel. The tissue structural image is identical to the conventional OCT image, delineating the typical morphological features of the LN and its surrounding adipose tissue [Fig. 1(a)], while the blood flow in the patent microvessels is localized at depths of ~1.0 mm through the lymphatic tissue [Fig. 1(b)]. The rich capillary vessels could be resolved, particularly within the cortex region of the LN (e.g., pointed by arrows). The 3-D optical dataset containing both the morphological and blood flow information can be manipulated to display enface tissue slices at particular depths, one example of which is shown in Figs. 1(c) and 1(d), respectively, illustrating the spatial relationship between the vasculature and tissue microstructures at a depth location of ~400 μm beneath the surface. Here, with reference to the standard LN histopathology,[12] the high endothelial venues (HEVs) typically presented in the medulla draining the blood into the large collecting vein can be identified. The LN arteriole and dense capillary beds (pointed by arrows) are also seen.

Figure 2 gives volumetric visualization of the scanned tissue volume to better appreciate how the vasculature network innervates the lymphatic tissue. Analyses of morphological features of blood vessels and microstructures of the LN afforded by the 3-D OMAG dataset provide detailed information about blood flow in both lymphatic tissue volumes and individual blood vessels. UHS-OMAG thus may be a useful tool for investigations of potential mechanisms of the normal LN physiological functions as well as their responses to the therapeutic treatment under diseased conditions, e.g., inflammation and cancer.UHS-OMAG is superior in visualizing complex morphological features and blood vessel networks deeper (>1000 μm) within the LNs.

Because the lymph fluid appears almost transparent optically, a recent report has shown that the negligible OCT scattering intensity from the lymph fluid can be utilized to delineate lymph vessel networks, which innervates the scanned

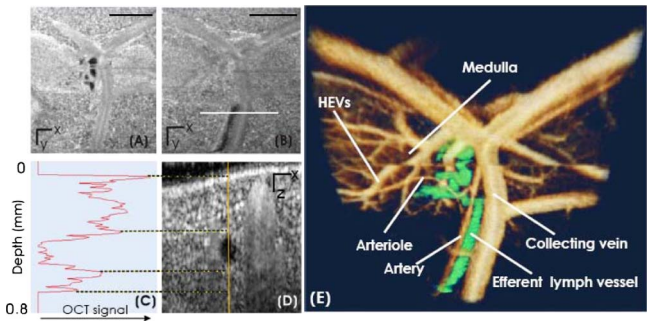

Fig. 3 UHS-OMAG has the potential to identify both the vasculatures and lymphatic vessels within axillary lymph nodes, without the need of a contrast agent. (a) and (b) show the enface structural images of lymph node at depths of ~200 and ~400 μm, respectively. (Scale bar: 500 μm). (d) is a cross sectional image of microstructures taken at the location indicated by the white line in (b), where the black hole is assumed to be a lymphatic vessel, and (c) shows the profile of optical scattering strength from top to bottom, as indicated by the line. (e) gives the 3-D view of the merged vasculature and lymphatic vessels (green color). The volume size is $2.0\times2.0\times1.5$ mm^3 (x-y-z). (Color online only.)

tissue volume *in vivo*.[13] Being an extension of OCT technology, UHS-OMAG is also able to extract the information about the lymph vessels within LNs, and that can be coregistered perfectly with the lymphatic tissue morphology and vasculature. One such example is shown in Fig. 3, where the enface structure images of an axillary LN are shown at depths of ~200 [Fig. 3(a)] and 400 μm [Fig. 3(b)], respectively, along with a cross sectional tissue slice across a lymph vessel [Fig. 3(d)]. Dark areas [low scattering region, e.g., in Fig. 3(c)] observed from the OMAG microstructure images were due to the lymph fluid in the patent lymph vessels. According to this feature, an automatic algorithm was developed to segment the lymph vessels from the 3-D OMAG dataset by setting a fixed intensity threshold to transform the 3-D images into binary format. After segmentation, the lymphatic network was merged with the vasculature network, illustrating the relationship between the blood and lymph vessels. The result is shown in Fig. 3(e), where the efferent lymph vessel is seen almost parallel to the large collecting vein, with the LN vasculature appearance similar to that in Figs. 1 and 2. Without the need for exogenous contrast agents, UHS-OMAG may have potential to monitor functional lymphatic and blood vessels within the LNs. Notably, the OMAG lymphangiography can be performed simultaneously with the tissue morphology and vascular microangiography, and these can be done from one single OMAG volumetric scan.

One difficulty with UHS-OMAG when it requires deeper imaging within lymphatic tissue is its poor penetration depth in tissue, which is typically limited to one transport mean-free path length (~1.5 mm). Therefore, the current study required US to surgically expose the axillary lymph nodes for UHS-OMAG imaging. However, reports have shown that an OCT probe can be miniaturized and encased in a medical needle.[14] Such an imaging probe could be integrated with OMAG to interstitially image the LNs *in vivo*. In addition, further improvement of the system resolution (currently ~9 μm) is also necessary to facilitate the accurate segmentation of detailed lymphatic vessels from the 3-D microstructural images. Furthermore, in the current study, we assume that lymph fluid is transparent, which gives us the opportunity to extract lymph vessel within the scanned tissue volume. This assumption needs further experimental validation through a correlation study of OCT images with histopathological preparation.

In summary, we demonstrate the ability of UHS-OMAG to provide detailed morphology, and microvasculature, as well as lymphatic vessels within intact axillary lymph nodes. The results suggest that, by using OMAG, it could be feasible to visualize the lymphatic tissue morphology and to monitor changes in blood and lymph microcirculations, thus offering potential for assessing LN involvement in diseased conditions, as well as for monitoring the dynamic responses of the microvascular and lymphatic vessels to therapeutic treatment *in vivo*.

This work was supported in part by research grants from the National Institutes of Health (R01HL093140, R01EB009682, and R01DC010201), and the American Heart Association (0855733G).

References

1. P. Veronesi, G. Paganelli, V. Galimberti et al., "Sentinel-node biopsy to avoid axillary dissection in breast cancer with clinically negative lymph-nodes," *Lancet* **349**, 1864–1867 (1997).
2. D. Krag, D. Weaver, T. Ashikaga et al., "The sentinel node in breast cancer—a multicenter validation study," *N. Engl. J. Med.* **339**, 941–946 (1998).
3. A. D. Purushotham, S. Upponi, M. B. Klevesath, L. Millar, J. Peter Myles, and S. W. Duffy, "Morbidity after sentinel lymph node biopsy in primary breast cancer: results from a randomized controlled trial," *J. Clin. Oncol.* **23**, 4312–4321 (2005).
4. L. V. Wang, "Prospects of photoacoustic tomography," *Med. Phys.* **35**, 5758–5767 (2008).
5. T. Erpelding, C. Kim, M. Pramanik, L. Jankovic, K. Maslov, Z. Guo, J. A. Margenthaler, M. D. Pashley, and L. V. Wang, "Sentinel lymph nodes in the rat: Noninvasive photoacoustic and US imaging with a clinical US system," *Radiology* **256**, 102–110 (2010).
6. W. Luo, F. T. Nguyen, A. M. Zysk, T. S. Ralston, J. Brockenbrough, D. L. Marks, A. L. Oldenburg, and S. A. Boppart, "Optical biopsy of lymph node morphology using optical coherence tomography," *Technol. Cancer Res. Treat.* **4**, 539–548 (2005).
7. R. A. McLaughlin, L. Scolaro, P. Robbins, S. Hamza, C. Saunders, and D. D. Sampson, "Imaging of human lymph nodes using optical coherence tomography: potential for staging cancer," *Cancer Res.* **70**, 2579–2584 (2010).
8. R. K. Wang, S. L. Jacques, Z. Ma, S. Hurst, S. R. Hanson, and A. Gruber, "Three dimensional optical angiography," *Opt. Express* **15**, 4083–4097 (2007).
9. L. An, J. Qin, and R. K. Wang, "Ultrahigh sensitive optical microangiography for *in vivo* imaging of microcirculations within human skin tissue beds," *Opt. Express* **18**, 8220–8228 (2010).
10. Y. L. Jia, L. An, and R. K. Wang, "Label-free and highly sensitive optical imaging of detailed microcirculation within meninges and cortex in mice with the cranium left intact," *J. Biomed. Opt.* **15**, 030510 (2010).
11. R. K. Wang, L. An, P. Francis, and D. J. Wilson, "Depth-resolved imaging of capillary networks in retina and choroid using ultrahigh sensitive optical microangiography," *Opt. Lett.* **35**, 1467–1469, (2010).
12. C. L. Willard-Mack, "Normal structure, function, and histology of lymph nodes," *Toxicol. Pathol.* **34**, 409–424 (2006).
13. B. J. Vakoc, R. M. Lanning, J. A. Tyrrell, T. P. Padera, L. A. Bartlett, T. Stylianopoulos, L. L. Munn, G. J. Tearney, D. Fukumura, R. K. Jain, and B. E. Bouma. "Three-dimensional microscopy of the tumor microenvironment *in vivo* using optical frequency domain imaging," *Nat. Med.* **15**, 1219–1223 (2009).
14. X. Li, C. Chudoba, T. Ko, C. Pitris, and J. G. Fujimoto, "Imaging needle for optical coherence tomography," *Opt. Lett.* **25**, 1520–1522 (2000).